THE SUITABILITY OF CLEAR SKY DIFFUSE IRRADIANCE MODELS FOR SOUTH AFRICAN ATMOSPHERIC CONDITIONS

Hartmut Winkler[1]

[1] Department of Physics, University of Johannesburg, PO Box 524, 2006 Auckland Park, Johannesburg, South Africa; Phone: +27-11-5594417; Fax: +27-11-5592339; E-Mail: hwinkler@uj.ac.za

Abstract

This paper examines the suitability of various diffuse irradiance models to reproduce clear sky irradiance characteristic of South Africa. Diffuse component daily profiles determined from various theoretical models are compared to actual South African diffuse irradiance data collected in De Aar in 2000, for which local sky characteristics and aerosol concentration and composition above the site are precisely known. Four cases are explored, corresponding to (i) an aerosol-free atmosphere, (ii) the presence of atmospheric layers of evolved biomass-burning aerosols, (iii) low-level aeolian dust and (iv) particles associated with anthropogenic activity. It is found that both the integrated and spectral diffuse horizontal irradiance can, when conditions remain stable, be extremely well represented by simple mathematical relationships such as power laws and third-order polynomials. Theoretical models are generally unable to reproduce the diffuse irradiance/solar zenith angle relationship as well. If suitably adapted to specific site altitude, such fits provide an ideal diffuse irradiance determination for site-specific solar potential studies, even under occasional conditions of higher than normal aerosol loading.

Keywords: Solar irradiance; diffuse irradiance; turbidity; South Africa.

1. Introduction

The electricity generating potential of photovoltaic devices in part depends on the scattered skylight (also referred to as diffuse irradiance) incident on a module. The sky irradiance is particularly difficult to model, as it is the superposition of photons that underwent one or more scattering events whose characteristics depend on a large variety of parameters related to the following: particle concentrations, particle size distributions, reflective properties (all of these being also wavelength dependent) and solar position.

Models produced by various researchers have evolved from an original uniform sky brightness model to modern ones involving sophisticated multi-function fitting of various parameters. The suitability of these models to describe a typical South African sky (usually with low aerosol concentrations, mostly at high altitude sites) has not been verified extensively. This paper seeks to test some models on South African diffuse irradiance data and pronounce on these models' applicability, and thus determine their suitability for local site irradiance calculations.

While extensive solar irradiance models exist that have proved excellent in describing the insolation in many places around the world, atmospheric conditions in the interior of South Africa are not necessarily best described by the parameterisation adopted in these models [1]. So local validation of irradiance models remains important.

2. Diffuse irradiance models

2.1. Diffuse irradiance

Solar photons reaching a measuring device along a solar beam without deflection are collectively referred to as direct radiation. When measured in terms of total photon energy per second per wavelength interval passing through a unit area perpendicular cross section, this is quantified as the direct normal spectral irradiance I_λ. The direct normal irradiance I is therefore

$$I = \int_{\text{all}\lambda} I_\lambda d\lambda \, .$$

Diffuse radiation is defined as any solar light incident on a surface that is not part of the direct beam. It is made up of all solar photons scattered in the atmosphere towards the detector. As with the direct portion, diffuse light can be quantified in terms of photon energy per second per wavelength interval incident on a unit area. When this receiving area is horizontal, this is referred to as the diffuse horizontal spectral irradiance D_λ. The diffuse horizontal irradiance is therefore

$$D = \int_{\text{all}\lambda} D_\lambda d\lambda \, .$$

Combined with a solar energy generating device's geometric (orientation) and instrumental (spectral sensitivity) parameters, these quantities determine the amount of solar radiation converted into electricity.

2.2. Key irradiance parameters

For setups where the detector is a horizontal surface, geometric effects are adequately described by one positional parameter only, the solar zenith angle ζ.

The formalism introduced in the following paragraphs has been used in a vast number of studies, of which a few of the better-known ones are listed here [2] [3] [4] [5]. It should be noted that the notation used in these numerous works is by no means uniform.

The direct solar beam is subject to attenuation in the atmosphere. The form of the attenuation is best described by a Beer-Lambert law as given below, where $I_{S\lambda}$ represents the solar spectral irradiance at the top of the atmosphere.

$$I_\lambda = I_{S\lambda}\exp(-\tau_\lambda \sec\zeta)$$

The parameter τ_λ is referred to as the optical depth. It is a measure of the degree of atmospheric turbidity. It common to write this parameter as the sum of the optical depths associated with different atmospheric components:

$$\tau_\lambda = \tau_{r\lambda} + \tau_{a\lambda} + \tau_{g\lambda}$$

The first of these, with the subscript "*r*", is associated with Rayleigh scattering. This is the process where photons are deflected by the smallest particles. In the case of a typical atmosphere these particles are those making up the air. The Rayleigh optical depth is therefore only dependent on the amount of air above a site. This is proportional to the site atmospheric pressure, which is only weakly variable, and is therefore basically just a function of site height above sea level.

The second term, $\tau_{a\lambda}$, is the aerosol optical depth. It is determined by the Mie scattering of photons off aerosols, i.e. larger particles suspended in the air. These may arise from smoke, wind-generated dust, volcanic ash and a range of less common processes, all of which result in increased haze and turbidity. The wavelength dependence of the aerosol optical depth is usually well described by the form

$$\tau_{a\lambda} = \beta\lambda^{\alpha(\lambda)}$$

where α and β are referred to as the Ångstrom parameters. Usually the α parameter (also called the Ångstrom exponent) itself exhibits a mild dependence on wavelength. Therefore, its derivative with respect to $\ln\lambda$, α', is also sometimes measured [6].

The third term, $\tau_{g\lambda}$, constitutes the optical depth due to several specific gases usually present in the atmosphere. These include ozone, water vapour and nitrogen, for which detailed parameterisation procedures have previously been developed [4]. This gas optical depth only affects those parts of the spectrum that coincide with a particular gas' spectral lines. It can be omitted when one is specifically considering parts of the spectrum containing no such spectral features.

When sunlight is recorded on a ground-level horizontal surface, the measured spectral irradiance, in this case termed global horizontal spectral irradiance G_λ, will be a combination of the angle-corrected direct normal spectral irradiance and the diffuse spectral horizontal irradiance:

$$G_\lambda = I_\lambda \cos\zeta + D_\lambda \,.$$

The definition of the integrated global horizontal irradiance is correspondingly therefore defined by

$$G = I\cos\zeta + D \,.$$

As solar modules are usually not horizontal but tilted, these quantities ultimately need to be converted to these different configurations.

2.3. Common diffuse irradiance models

There have been two approaches to modelling diffuse irradiance.

The first of these is a theoretical approach that attempts to incorporate as many physical processes as possible in the model to improve the match of increasingly sophisticated theoretical relationships to the data. In view of the complexities inherent in the multiple concurrent processes, this has proved difficult.

The second approach is to determine empirical fits to plots of relationships between the diffuse irradiance and other quantities. It is often possible to do so to a high degree of accuracy using surprisingly simple mathematical expressions.

The models in sections 2.3.1 and 2.3.2, as well as many related variants, follow the theoretical approach. The remaining sub-sections describe empirical solutions.

2.3.1. Suckling-Hay and related models

Models in this class [7] were originally based on the simplifying assumptions that there is only one scattering event per photon and that exactly half of the scattered photons reach the ground (while the remaining half exit the atmosphere after being scattered upward). In its most straightforward form,

$$D = \tfrac{1}{2} I_S \cos\zeta\,[1-\exp(-\tau\sec\zeta)] \,.$$

Given that τ is actually strongly wavelength dependent, and as aerosols preferentially scatter in a forward direction, this formulation is only expected to match real data very crudely.

2.3.2. Bird-Riordan and related models

These models for the spectral diffuse horizontal irradiance are based on the same thought process that led to the models in section 2.3.1. There is here however a realisation that Rayleigh

and aerosol scattering should be treated separately (as aerosols normally exhibit a forward directional bias).

The most quoted formulation is that due to Bird and Riordan [2], which developed from earlier attempts by Leckner [8] and Justus and Paris [9], with which the Bird-Riordan model shares considerable commonalities. The basic idea is that, if secondary scattering is ignored, half of the photons scattered in the atmosphere will make their way to the ground and get recorded as diffuse radiation.

In parts of the spectrum unaffected by gas-induced spectral losses, the diffuse spectral horizontal irradiance is in this model described by the expression

$$D_\lambda = \tfrac{1}{2} I_{S\lambda}\cos\zeta\,[1-\exp(-x\,\tau_{r\lambda}\sec\zeta)]$$

$$+ F\times I_{S\lambda}\cos\zeta\exp(-y\,\tau_{r\lambda}\sec\zeta)\times[1-\exp(-\tau_{a\lambda}\sec\zeta)]$$

where the unspecified parameters proposed by Bird and Riordan were $x = 0.95$, $y = 1.5$ [2]. The parameter F is the fraction of radiation scattered downwards due to aerosols.

2.3.3. Ineichen model

The diffuse horizontal irradiance formulation introduced here appears to have similarities to the earlier models in that there is here too an exponential decline term that is a function of $\sec\zeta$. The power exponent parameter d however places this into the category of empirical models. This mathematically straightforward formulation, here named after the study that apparently first suggested it [10], gives D as

$$D = D_0 \exp(\tau_d)\exp(-\tau_d \sec^d\zeta)\,.$$

D_0 is here the diffuse horizontal irradiance for $\zeta = 0$. Ineichen [10] proposed the following values for the other parameters: $\tau_d = 2.698$ and $d = 0.187$. It could however be that different values for these parameters would be more appropriate in other environments.

2.3.4. Power law model

The empirical power law relationship between D and $\cos\zeta$ has already been commented on in many previous studies [11] [12]. It may be formulated as

$$D = D_0\,(\cos\zeta)^q$$

where q an arbitrary the power law exponent.

The simplicity of this approach, combined with its excellent approximation of the diffuse irradiance-zenith angle relationship, makes the use of this model an attractive proposition.

2.3.5. Polynomial model

While polynomials can be employed to fit most natural data, what makes this formulation practical is that for stable atmospheric conditions the diffuse spectral irradiance can be matched exceptionally closely by a polynomial of only third order, and in some instances even second order (i.e. $c_3 = 0$):

$$D_\lambda = c_{0\lambda} + c_{1\lambda}\cos\zeta + c_{2\lambda}\cos^2\zeta + c_{3\lambda}\cos^3\zeta\,.$$

Such a relatively simple expression is very helpful when engaging in computational work.

3. Data analysis

3.1. Sunphotometry data from De Aar

A YESDAS rotating shadowband sunphotometer was in operation at the South African Weather Services station in De Aar, Northern Cape, between July 2000 and February 2001.

The findings of the analysis of data collected over this period were published in a previous study [13]. Amongst other things, those investigations determined the aerosol characteristics in the atmosphere above the site.

For this study, a set of days and their corresponding data were identified that had previously been shown to be good representations of specific aerosol aggregations. These are identified in Table 1, together with one of the aerosol optical depths, the Ångstrom exponent and its derivative.

Date	Aerosol type	τ_a(415nm), α, α'
1 Aug 2000	aeolian dust	0.126, 1.66, –0.98
4 Aug 2000	very low aerosols	0.013, – , –
8 Aug 2000	biomass burning	0.225, 1.92, 0.69
21 Sep 2000	anthropogenic	0.123, 1.51, 0.25

Table 1. Days investigated and aerosol characteristics on those days from Winkler et al. [13]

The diffuse measurements obtained on these days are examined in this paper.

3.2 The diffuse irradiance data

The data sets for the days listed in Table 1 include minute-by-minute relative diffuse irradiances through three narrow band filters centred at 415 nm, 501 nm and 868 nm. Except for a weak effect by ozone on the 501 nm band, these readings are not affected by spectral lines associated with gas molecules.

The Rayleigh optical depths used for De Aar relating to the narrow band filters examined here were as follows: $\tau_{r,415nm} = 0.267$, $\tau_{r,501nm} = 0.123$ and $\tau_{r,868nm} = 0.013$.

The daily diffuse irradiance light curves measured (both broad band and for the three narrow bands) for two of the days are displayed in Figs 1 and 2.

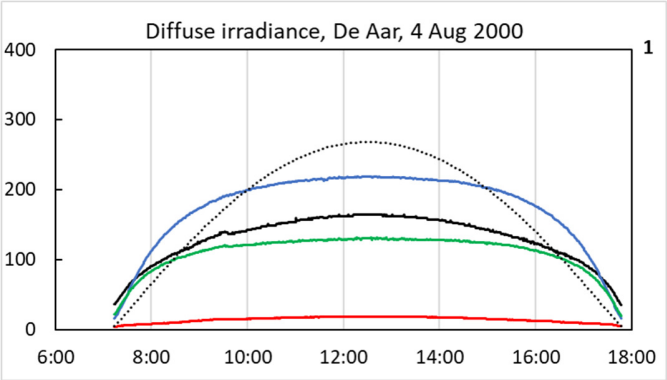

Fig. 1. The diffuse irradiance measured over the time of day on 4 Aug 2000, when aerosol concentrations were very low. The blue, green and red curves (left vertical scale, in $W.m^{-2}.nm^{-1}$) represent the 440 nm, 501 nm and 868 nm bands respectively. The black curve traces the broad-band diffuse irradiance (relative to the maximum on 8 Aug, right vertical scale). The dotted line plots $\cos\zeta$, to illustrate the poor diffuse component match to that function.

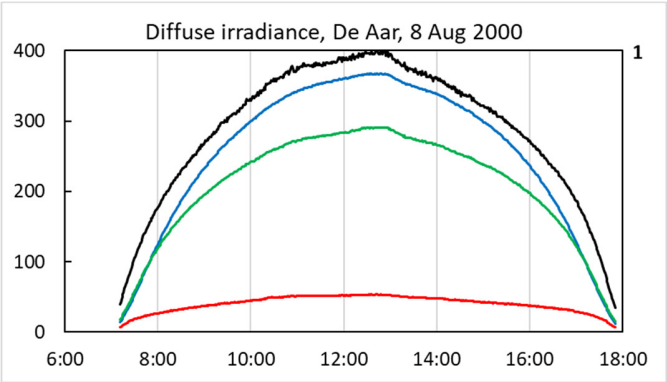

Fig. 2. Diffuse irradiance measurements for 8 Aug 2000, when aerosol concentrations were high. The curve colour codes and *y*-scale are the same is in Fig. 1.

3.3. Fitting the diffuse irradiance curves

The $\cos\zeta$ and $\sec\zeta$ terms common to all models suggest that plots of D vs. $\cos\zeta$ would be the most insightful. Such plots are shown in Fig. 3.

Both the anthropogenic and aeolian dust curves display signs of unevenness presumably occasioned by intra-day variations in the aerosol concentration. This is not unexpected in low-level aerosol layers where little mixing has occurred. Unlike the low aerosol and biomass burning plots, the curves for these aerosol types are therefore not well suited for testing high precision model fits.

The first observation made is that the Suckling-Hay-type curves fitted the diffuse horizontal irradiance curves very poorly. Typically, these curves badly underestimate D when the Sun nears the horizon. Furthermore, the curves corresponding to this model display a stronger curvature in the range $0.2 < \cos\zeta < 0.7$ than the actual data.

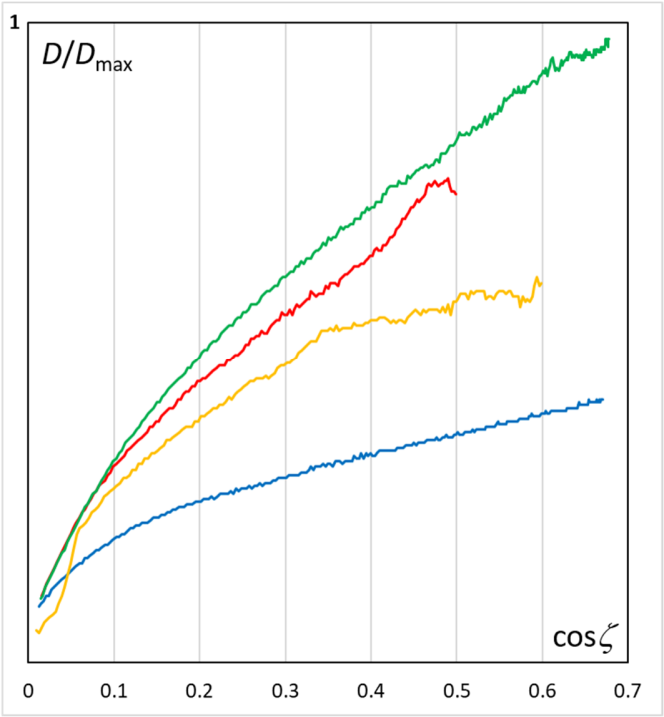

Fig. 3. The broad band diffuse irradiance vs. cos ζ curve. The curves are colour coded: very low aerosol (blue), anthropogenic (yellow), aeolian dust (red) and biomass burning (green).

The Ineichen and power law models fare much better. In Fig. 4, the actual data and Ineichen model curves are plotted relative to the power law model for the low aerosol and biomass burning scenarios. The power law model performs better overall (the R^2 correlation parameter is greater than 0.998 in both cases), but the Ineichen model provides a closer match in the range $0.05 < \cos\zeta < 0.45$.

In view of the poor characterisation of the aeolian dust and anthropogenic curves, the Ineichen model was only applied to the low aerosol and biomass burning scenarios. Suitable fits were obtained for the parameters listed in Table 2. Note that D_{r0} represents the diffuse $\zeta = 0$ case for Rayleigh scattering only, which is well approximated by the "very low aerosol" case.

Aerosol type	D_0/D_{r0}	τ_d	d
very low aerosols	1.0	2.8	0.110
biomass burning	2.3	2.7	0.165

Table 2. Ineichen model parameters determined for 4 and 8 August 2000 (low aerosol and biomass burning)

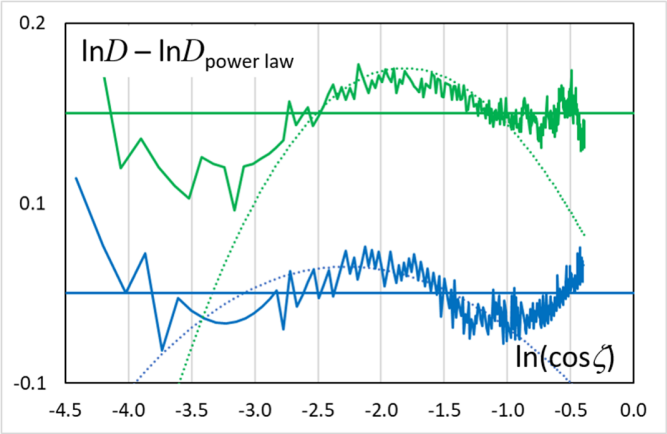

Fig. 4. Plot of ln$D$ vs. ln(cosζ) relative to a power law. The curves are colour coded: very low aerosol curves are in blue, while biomass burning is represented in green. The dotted curves are for the Ineichen model fits.

The optimal parameters for the power law fits are in turn listed in Table 3. A value is here also given for the aeolian dust case, using only the smoother section of the curve where cosζ < 0.5.

Aerosol type	D_0/D_{r0}	q
very low aerosols	1.000	0.396
aeolian dust	2.300	0.563
biomass burning	2.622	0.601

Table 3. Diffuse irradiance D vs cosζ power law fit

None of the parameters listed in Tables 2 and 3 exhibit any obvious proportionality relationship with the optical depths (total or aerosol) measured for the days in question.

3.4. Fitting the diffuse spectral irradiance curves

The diffuse spectral irradiance plots are shown in Figs. 5 and 6.

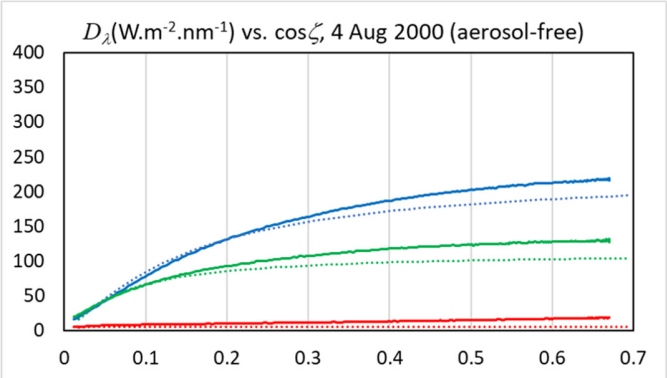

Fig. 5. The 415 nm (blue), 501 nm (green) and 868 nm (red) plots of D_λ vs. cosζ for 4 August 2000. The dotted lines are the Bird-Riordan model fits with F = 0.75.

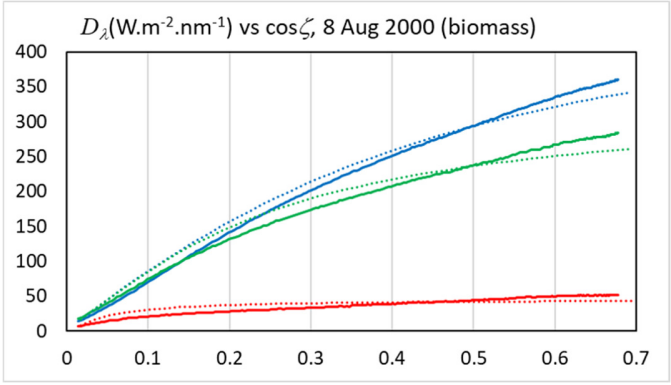

Fig. 6. The 415 nm (blue), 501 nm (green) and 868 nm (red) plots of D_λ vs. cosζ for 8 August 2000, when there were high aerosol concentrations induced by biomass burning. Again, the dotted lines are the Bird-Riordan model fits.

Also shown in these diagrams (using dotted lines) are the diffuse spectral horizontal irradiance curves calculated with a Bird-Riordan model using F = 0.75. These model curves underestimate the diffuse contribution for the aerosol-free scenario. They match the measured data better for the higher aerosol concentrations associated with biomass burning on 8 Aug 2000. The shapes of the curve are however such that the diffuse component is overestimated when the Sun is low on the horizon and underestimated at small solar zenith angles.

The polynomial curves instead provided a much closer fit to the data. The optimal polynomial coefficients are listed in Table 4.

Aerosol type	λ(nm)	c_0 (W.m^{-2}.nm^{-1}), c_1, c_2, (c_3)
very low aerosols	415	5.197, 848.0, –1256, 695.7
	501	19.46, 530.0, –949.5, 607.8
	868	6.033, 24.02, –23.67, 24.48
aeolian dust	415	3.528, 768.7, –428.2, (0)
	501	19.14, 576.6, –380.6, (0)
	868	10.80, 75.26, –31.12, (0)
biomass burning	415	–4.218, 826.8,–534.4, 158.9
	501	4.841, 781.3, –872.6, 486.8
	868	9.085, 122.0, –156.0, 106.6
anthropogenic	415	3.816, 812.7, –631.9, (0)
	501	24.57, 548.6, –478.5, (0)
	868	11.03, 60.44, –51.72, (0)

Table 4. Polynomial fit coefficients of the spectral diffuse horizontal irradiance curves for different aerosol types.

Because of the unevenness of the aeolian wind and anthropogenic curves, the cubic term was excluded for these. It is worth noting that a quadratic polynomial would also have led to exceptionally good matches in the biomass burning graph.

Table 5 explores the relationship between the diffuse component brightness and direct beam losses as measured by the optical depth.

Aerosol type	λ (nm)	very low aerosols	biomass burning
$D_{\lambda 0}$	415	292.9	448.1
($W.m^{-2}.nm^{-1}$)	501	207.8	400.4
	868	30.9	81.7
$(D_{\lambda 0}-D_{\lambda r0})/\tau_{a\lambda}$	415	[1100]	690
$[D_{\lambda 0}/\tau_{r\lambda}$ for "very low aerosol"]	501	[1690]	1230
	868	[2400]	930

Table 5. Relationship between diffuse spectral irradiance and optical depth.

While there is as expected a strengthening of the diffuse contribution when skies are more turbid, no linear relationship is evident between these.

4. Discussion

Given the contribution of the diffuse irradiance component to the total light collected by a solar module, its total amount, as well as its spectral and angular distribution, should be accurately known to determine the actual amount of power generated by the module. A well determined sky contribution is also necessary to model the optimal solar module configuration.

The suitability of the various models to fit the diffuse component data assumed to be typical of South African conditions is summarised in Fig. 7. Even with different parameters, the Suckling-Hay and Bird-Riordan models are unable to replicate the overall shape of the measured diffuse irradiance-zenith angle relationship, while the mathematical fits using a power law (for diffuse irradiance) or third-order polynomial (for diffuse spectral irradiance) are able to match the curves best.

The empirical fits developed here fit the diffuse irradiance profiles exceptionally well. The parameters determined here for aerosol-free conditions in De Aar, which has four operational solar farms in its immediate neighbourhood, provide an accurate characterisation of diffuse irradiance at this location for much of the year. This is because enhanced aerosol conditions (in otherwise clear conditions) are comparatively uncommon over much of the western South African interior [13].

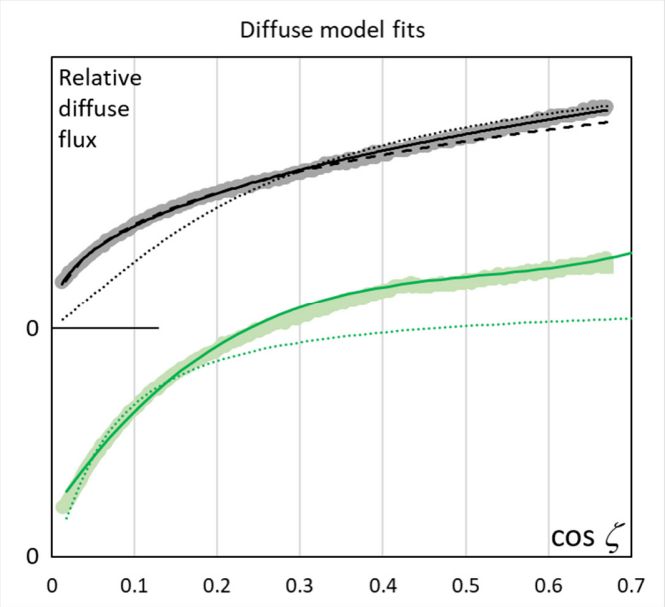

Fig. 7. The broad band diffuse irradiance (black) and 501 nm spectral irradiance (green) vs. cos ζ curve. The shaded area marks the 4 Aug 2000 measured data. The solid curves are the power law and polynomial fits. The dashed line is the Ineichen model, and the dotted lines are the Suckling-Hay and Bird-Riordan model curves respectively.

Increased turbidity events are most common in spring, before the start of the summer rainfall season. In most instances these events are due to biomass burning aerosols [13]. While the fit parameters were determined for only one such event, it would be possible to extend the work done here to determine a general relationship between these parameters and the aerosol optical depth suitable for De Aar and other South African sites at similar altitude above sea level.

In view of the stability of the processes related to Rayleigh scattering, it would furthermore be possible to repeat the investigation performed here for sites at different altitudes, and determine a relationship between the diffuse irradiance profile parameters and altitude above sea level.

How do these findings then lead to the determination of solar energy yield for specific solar module configurations at arbitrary South African sites? To determine the power generated by a horizontal solar module at any specific time of the day, the following calculation must be applied:

$$P = A \int (I_\lambda \cos\zeta + D_\lambda)\phi(\lambda)d\lambda$$

where A is the solar module area and $\phi(\lambda)$ is the specific solar module's spectral response function. Where only integrated irradiance quantities G, I and D are known, this operation cannot be performed exactly, and any calculations involving empirically determined correction factors are highly dependent on the nature

of $\phi(\lambda)$.

Solar modules are furthermore in most instances tilted away from the vertical. They may also be turned away from a north-facing direction, which is normally assumed to be the optimal bearing. To correct for these orientational effects, a range of models have been established [14], including the popular formulations developed by Perez and collaborators [15].

5. Conclusion

Integrated and spectral diffuse horizontal irradiance measurements made at a typical South African site were tested against a variety of theoretical models and empirical fitting procedures. The empirical fits always provided a much closer match to the relationships between the diffuse irradiance and the solar zenith angle.

Acknowledgements

The author acknowledges funding from the NRF. The instrument on which the data was collected in 2000 belonged to the Max Planck Instutut für Chemie in Mainz, Germany, and the SAWS are again thanked for making their De Aar facility available for data collection. The measurement programme in 2000-2001 was co-managed with extensive support from Dr Paola Formenti and the late Danie Esterhuyse.

References

[1] H. Winkler, (2017) Proceedings of the 2016 Annual Conference of the South African Institute of Physics, 4-8 Jul 2016, Cape Town, 439-444

[2] R.E. Bird, C. Riordan, Journal of Climate and Applied Meteorology, 25 (1986) 87-97.

[3] C. Rigollier, O. Bauer, L. Wald, Solar Energy, 68 (2000) 33-48.

[4] C.A. Gueymard, Solar Energy, 71 (2001) 325-346.

[5] J. Hofierka, M. Šuri, Proceedings of the Open source GIS-GRASS users conference 2002, Trento, Italy (2002) 1-19.

[6] T.F. Eck, B.N. Holben, J.S. Reid, et al., Journal of Geophysical Research, D24 (1999) 31333-31349.

[7] P.W. Suckling, J.E. Hay, Atmosphere, 14 (1976), 298-308.

[8] B. Leckner, Solar Energy, 20 (1978), 143-150.

[9] C.G. Justus, M.V. Paris, Journal of Climate and Applied Meteorology, 24 (1985) 193-205.

[10] P. Ineichen, Solar Energy, 82 (2008) 758-762.

[11] M.J. Reno, C.W. Hansen, J.S. Stein, (2012) Global horizontal irradiance clear sky models: implementation and analysis, Report SAND2012-2389, Sandia National Laboratories

[12] J. Bilbao, R. Román, C. Yousif, et al., Energy Procedia, 57 (2015) 1206-1210.

[13] H. Winkler, P. Formenti, D.J. Esterhuyse, et al., Atmospheric Environment, 42 (2008) 5569-5578.

[14] E.G. Esveev, A.I. Kudish, Solar Energy, 83 (2009) 377-388.

[15] R. Perez, R. Stewart, C. Arbogast, et al., Solar Energy, 32 (1986) 481-497.